JOURNAL OF CATALYSIS **180,** 207–217 (1998)
ARTICLE NO. CA982264

Rhodium Supported on Faujasites: Effects of Cluster Size and CO Ligands on Catalytic Activity for Toluene Hydrogenation

W. A. Weber and B. C. Gates[1]

Department of Chemical Engineering and Materials Science, University of California, Davis, California 95616

Received April 6, 1998; revised August 21, 1998; accepted August 24, 1998

NaY zeolite-supported rhodium carbonyls, with the predominant species being $[Rh_6(CO)_{16}]$, were prepared by carbonylation of adsorbed $[Rh(CO)_2(acac)]$ at 125°C. The zeolite-supported rhodium carbonyl clusters were treated in He or in H_2 at 200, 250, or 300°C to remove the carbonyl ligands. When the decarbonylation took place in He, the resultant clusters had Rh–Rh coordination numbers (determined by extended X-ray absorption fine structure spectroscopy) between 3.5 and 3.9, with hardly any evidence of Rh–C contributions, indicating that the rhodium cluster frames were nearly intact and that decarbonylation was nearly complete. In contrast, when the treatment took place in H_2, partially decarbonylated rhodium clusters and aggregates formed, having Rh–Rh coordination numbers between 3.8 and 6.7; the rhodium aggregation increased with increasing temperature. The clusters formed by treatment in He at 200, 250, or 300°C all had similar catalytic activities for toluene hydrogenation. In contrast, the catalytic activities of the clusters and aggregates (partially decarbonylated at temperatures <300°C) formed in the presence of H_2 showed a strong dependence on treatment temperature, which is explained by inhibition by the remaining CO ligands and by cluster and aggregate size effects, with the aggregates being more active than the smaller clusters. Comparison of the data with those reported separately for rhodium clusters in NaX zeolite shows that NaY and NaX zeolites were nearly equivalent as supports. Comparison of the data with separately reported data indicates that the rhodium clusters are approximately the same in activity as iridium clusters of nearly the same size in NaY zeolite.

INTRODUCTION

Supported metal clusters consisting of only a few atoms each, illustrated by the platinum clusters in zeolite LTL [used commercially for naphtha reforming (1)], are intermediate in character between molecular metal complexes and bulk metal and might be expected to offer new catalytic properties. This expectation is largely untested, as this group of supported clusters is restricted to only a few metals [Ir (2–5), Pt (6), Os (7), and Ru (8)] and a few catalytic reactions, including hydrogenation of toluene and of CO (9–12) and hydrogenolysis of *n*-butane (13).

Here we extend this class of catalyst to rhodium, reporting the synthesis and structural characterization of zeolite-supported rhodium clusters and their catalytic activities for toluene hydrogenation. The results characterizing a family of zeolite-supported metal clusters provide a basis for comparison of the catalytic properties of rhodium clusters with those of iridium clusters of nearly the same size on the same support as well as a basis for comparison of the catalytic properties of rhodium clusters of nearly the same size on different zeolite supports.

EXPERIMENTAL METHODS

Materials

N_2, He (99.999%), CO (Puritan Bennett, UHP grade), and H_2 (99.99%, generated by electrolysis of water in a Balston generator) passed through traps containing particles of supported copper and zeolite to remove traces of O_2 and moisture, respectively. *n*-Pentane (Fisher, HPLC grade) was dried over sodium benzophenone ketyl and then deoxygenated by purging with flowing N_2 for 2 h. $[Rh(CO)_2(acac)]$[dicarbonylacetylacetonato rhodium (I)] (Strem, 99%) was used as received. NaY zeolite (without binder) [Davison Division of W. R. Grace and Co., Si : Al = 9.6 : 1 (atomic), average particle size = 5 μm] was calcined at 300°C in flowing O_2 for 4 h and then evacuated at 300°C for 12 h prior to use.

Preparation of Supported Rhodium Catalysts

All syntheses and sample transfers were conducted with exclusion of air and moisture on a double-manifold Schlenk vacuum line and in an N_2-filled Vacuum Atmospheres drybox. In each preparation, the zeolite support was brought in contact with a pentane solution of $[Rh(CO)_2(acac)]$ to yield a sample containing 2.3% Rh. The sample was slurried in dried *n*-pentane in a Schlenk flask under N_2 at room temperature for several days, and then the solvent was removed by evacuation and the solid dried *in vacuo* (pressure

[1] To whom correspondence should be addressed.

0021-9517/98 $25.00

$<10^{-3}$ Torr) overnight. The resulting solids were stored in the drybox for future experiments. Samples were carbonylated in a flow reactor with CO at 2 atm and subsequently decarbonylated in an EXAFS cell or in a flow reactor at 1 atm in either flowing H_2 or flowing He at temperatures of 200, 250, or 300°C for 2 h.

X-Ray Absorption Spectroscopy

To avoid air contamination, each sample to be characterized by X-ray absorption spectroscopy, while still in the drybox, was placed in a double layer of glass vials, each sealed with a vial cap and Parafilm. The sealed samples were placed in a glass desiccator and transported from the University of California, Davis, to the synchrotron.

The X-ray absorption experiments were performed on X-ray beamline X-11A at the National Synchrotron Light Source (NSLS) at Brookhaven National Laboratory, (Upton, NY) and on beamline 2–3 of the Stanford Synchrotron Radiation Laboratory (SSRL) at the Stanford Linear Accelerator Center (Stanford, CA). The storage ring operated at an energy of 2.5 GeV at NSLS and at an energy of 3 GeV at SSRL; the beam current was between 140 and 240 mA at NSLS and between 70 and 100 mA at SSRL.

Extended X-ray absorption fine structure (EXAFS) experiments in the transmission mode were carried out with wafers prepared in an N_2-filled glovebox at each synchrotron. A powder sample was placed in a holder in the glovebox, which was then placed in a die and pressed into a self-supporting wafer. The wafer was loaded into an EXAFS cell (14) and sealed. Typically, the cell was evacuated immediately after removal from the glovebox.

EXAFS spectra and X-ray absorption near edge spectra (XANES) were recorded for fresh and used catalysts formed by the decarbonylation of NaY zeolite-supported $[Rh_6(CO)_{16}]$. Samples were evacuated and cooled with liquid N_2; the sample temperature was approximately −150°C. Higher harmonics in the X-ray beam were minimized by detuning the Si(111) double-crystal monochromator at NSLS by 15–20% or the Si(220) double-crystal monochromator at SSRL by 15–20% at the Rh K edge (23220 eV).

Catalytic Hydrogenation of Toluene

The hydrogenation of toluene was catalyzed by NaY zeolite-supported rhodium in a once-through tubular flow reactor. To ensure high gas velocities and thorough mixing of gases, 40 mg of catalyst, initially consisting predominantly of $[Rh_6(CO)_{16}]$ in the zeolite (15), was diluted with 400 mg of inert α-Al_2O_3 particles and loaded into the reactor to give a catalyst bed about 2–3 mm in depth. The supported rhodium carbonyl precursors were treated in flowing He or H_2 to remove carbonyl ligands; the catalyst performance data characterize the decarbonylated (and partially decarbonylated) samples.

Toluene, injected into the flow system at a constant rate by an Isco 260D liquid metering pump, flowed to a vaporizer held at about 140°C. H_2 flowed through the vaporizer and was mixed with toluene; the gas mixture then passed through the reactor (mounted in a temperature-controlled electric furnace) at a total flow rate of 46 ml (NTP)/min. The effluent was analyzed with an on-line Hewlett–Packard gas chromatograph (HP-5890 Series II) equipped with a DB-624 capillary column (J&W Scientific) and a flame ionization detector. The catalytic activity was measured under the following conditions: partial pressures, $P_{H_2} =$ 710 Torr and $P_{toluene} = 50$ Torr; temperature = 80, 100, or 120°C.

Used catalyst samples prepared for EXAFS analysis were obtained by loading the reactor with 400 mg of catalyst in the absence of α-Al_2O_3; these samples were used to catalyze toluene hydrogenation at 100°C for 4 h on stream. The sealed reactor was transferred to the drybox, and the catalyst was removed and stored for transfer to a synchrotron.

Hydrogen Chemisorption

Hydrogen chemisorption measurements were performed with an RXM-100 multifunctional catalyst testing and characterization instrument manufactured by Advanced Scientific Designs, Inc., with a vacuum capability of 10^{-8} Torr. Each catalyst sample in the drybox (prior to decarbonylation) was loaded into a U-shaped quartz tube and sealed to prevent contamination during transfer to the chemisorption apparatus. Each sample was pretreated in flowing H_2 or He as the temperature was ramped at a rate of 3°C/min and held for 2 h at the temperature at which the sample had been previously treated in He or H_2 to remove carbonyl groups. The sample was then evacuated (10^{-7} Torr) at the treatment temperature and subsequently cooled to room temperature. It is possible that evacuation of the sample at the treatment temperature might have resulted in further decarbonylation of the sample if it had not already been fully decarbonylated. Adsorption isotherms were measured at 25°C and pressures in the range of 10–200 Torr. The amount of hydrogen irreversibly chemisorbed was measured as the difference between two consecutively measured isotherms (the total adsorption and the physical adsorption), with a 30-min evacuation between measurements. Accuracy in the determination of H/Rh values was ±0.01.

EXAFS DATA ANALYSIS

The EXAFS data were analyzed with experimentally determined reference files obtained from EXAFS data for materials of known structure (15), as described elsewhere (16). The analysis methods are described elsewhere (9, 15, 17).

RESULTS

Formation of Zeolite-Supported [$Rh_6(CO)_{16}$] and Subsequent Decarbonylation

When [$Rh(CO)_2$(acac)] was slurried with the calcined NaY zeolite in *n*-pentane solution, the solution became colorless, indicating uptake of the [$Rh(CO)_2$(acac)]. After removal of the solvent by evacuation, the resulting light gray solid was characterized by a ν_{CO} infrared spectrum with two strong bands (2082 and 2014 cm^{-1}), consistent with supported rhodium dicarbonyls, $Rh(I)(CO)_2$ (18–21). Treatment of the powder in flowing CO at 125°C for 12 h led to a light pink-gray solid with a ν_{CO} infrared spectrum (2130sh, 2092s, 2067sh, 2020w, 1765s cm^{-1}) consistent with those reported (22–25) for [$Rh_6(CO)_{16}$] in NaY zeolite; this cluster had evidently formed by reductive carbonylation (15).

When uncalcined NaY zeolite was used, the solution containing [$Rh(CO)_2$(acac)] was still faint yellow in color after stirring for 2 days. After removal of the solvent, the resulting solid was darker gray than the sample made from the calcined zeolite. Subsequent carbonylation gave [$Rh_6(CO)_{16}$], and the yield in the uncalcined zeolite was higher than that in the calcined zeolite (15).

Treatment of the supported rhodium carbonyl clusters in H_2 at 200°C for 2 h led to approximately 60–70% removal of the CO ligands (as estimated from the infrared band intensities). Treatment at 250°C in H_2 for 2 h led to increased decarbonylation, and treatment at 300°C led to nearly complete decarbonylation. In contrast, decarbonylation of the supported rhodium carbonyl clusters in He was nearly complete at only 200°C and complete at 250°C. The infrared spectra of the partially and fully decarbonylated clusters (15) were hardly dependent on the support pretreatment (calcination) temperature.

EXAFS Spectra of Partially and Fully Decarbonylated Rhodium Clusters

The raw EXAFS data characterizing the decarbonylated (or partially decarbonylated) rhodium clusters formed by the treatment of NaY zeolite-supported [$Rh_6(CO)_{16}$] in He (or in H_2) at 200, 250, or 300°C for 2 h (Samples 1–3 or Samples 4–6, respectively) show oscillations up to values of the wave vector *k* equal to about 15 $Å^{-1}$, consistent with Rh–Rh contributions and the presence of rhodium clusters (Fig. 1A). Standard deviations in the EXAFS function were less than 0.002 over the entire range of *k* space (about 4–16 $Å^{-1}$).

The EXAFS data characterizing rhodium clusters having few or no CO ligands, formed by treatment of zeolite-supported [$Rh_6(CO)_{16}$] in He (Samples 1–3), were fitted satisfactorily by a Rh–Rh contribution, at 2.69 Å, and Rh–low-*Z* contributions, approximated as a short Rh–O (2.1 Å) and a Rh–C contribution (1.95 Å) (Samples 1–3, Table 1). The Rh–C contribution may indicate the presence of by-products of decarbonylation, acac ligands, or products of acac decomposition. Details of the Rh–low-*Z* contributions are presented elsewhere (15). There was no significant change in the Rh–Rh first-shell coordination number as a result of increasing the temperature of treatment in He (200, 250, and 300°C); the values are 3.8, 3.5, and 3.9, respectively, all of which are barely distinguishable from the value observed for the precursor (3.2) (15)—within the expected experimental error (about ±20%) (Table 1).

In contrast, the EXAFS data representing the partially decarbonylated rhodium clusters (Samples 4–6, Table 1), formed by treatment of zeolite-supported [$Rh_6(CO)_{16}$] in H_2, were fitted satisfactorily by a Rh–Rh contribution, at 2.69 Å, and Rh–low-*Z* contributions, approximated as a short Rh–O (2.1 Å), a long Rh–O* (3.0 Å; O* refers to carbonyl oxygen), and a Rh–C contribution (1.95 Å) (Table 1). The clusters formed by treatment in H_2 at temperatures <300°C were characterized by Rh–C and Rh–O* contributions, indicating CO ligands, in agreement with the infrared spectra. The Rh–Rh first-shell coordination number characterizing the sample treated in H_2 at 200°C (Sample 4) was 3.5, which is indistinguishable from the precursor value (3.2) (Table 1), within the expected error. However, treatment of the sample in H_2 at 300°C resulted in a significant increase in the first-shell Rh–Rh coordination number, to 7.2, indicating the formation of rhodium that we refer to as aggregates (in contrast to the smaller clusters)—this was fully decarbonylated (Sample 6, Table 1). Details of the Rh–low-*Z* contributions are presented elsewhere (15).

To illustrate the goodness of the EXAFS data fits, comparisons of the raw data and the fits in *k* space and in *r* space (*r* is the distance from the absorber atom) are shown in Figs. 1A and 1B, respectively, for the aggregates formed by treatment of NaY zeolite-supported [$Rh_6(CO)_{16}$] in H_2 at 250°C. A comparison of the fitted Rh–Rh contribution with the residual spectrum formed by subtraction of the Rh–low-*Z* contributions from the raw EXAFS function is shown in Fig. 1C. Similarly, the fitted Rh–low-*Z* contributions [namely, the Rh–O_s (s denotes short), Rh–O*, and Rh–C contributions] are compared in Fig. 1D with the residual spectrum formed by subtraction of the Rh–Rh contribution from the raw EXAFS function. These comparisons show that both the Rh–Rh contributions and Rh–low-*Z* contributions were fitted satisfactorily.

To summarize, the results show that Samples 1, 2, 3, and 6 were fully or almost fully decarbonylated, whereas Samples 4 and 5 were only partially decarbonylated. Samples 1, 2, 3, and 4 are represented as clusters consisting of about 6 atoms each, on average. Samples 5 and 6 are represented as aggregates consisting of about 10 atoms and 50 atoms each, on average, respectively.

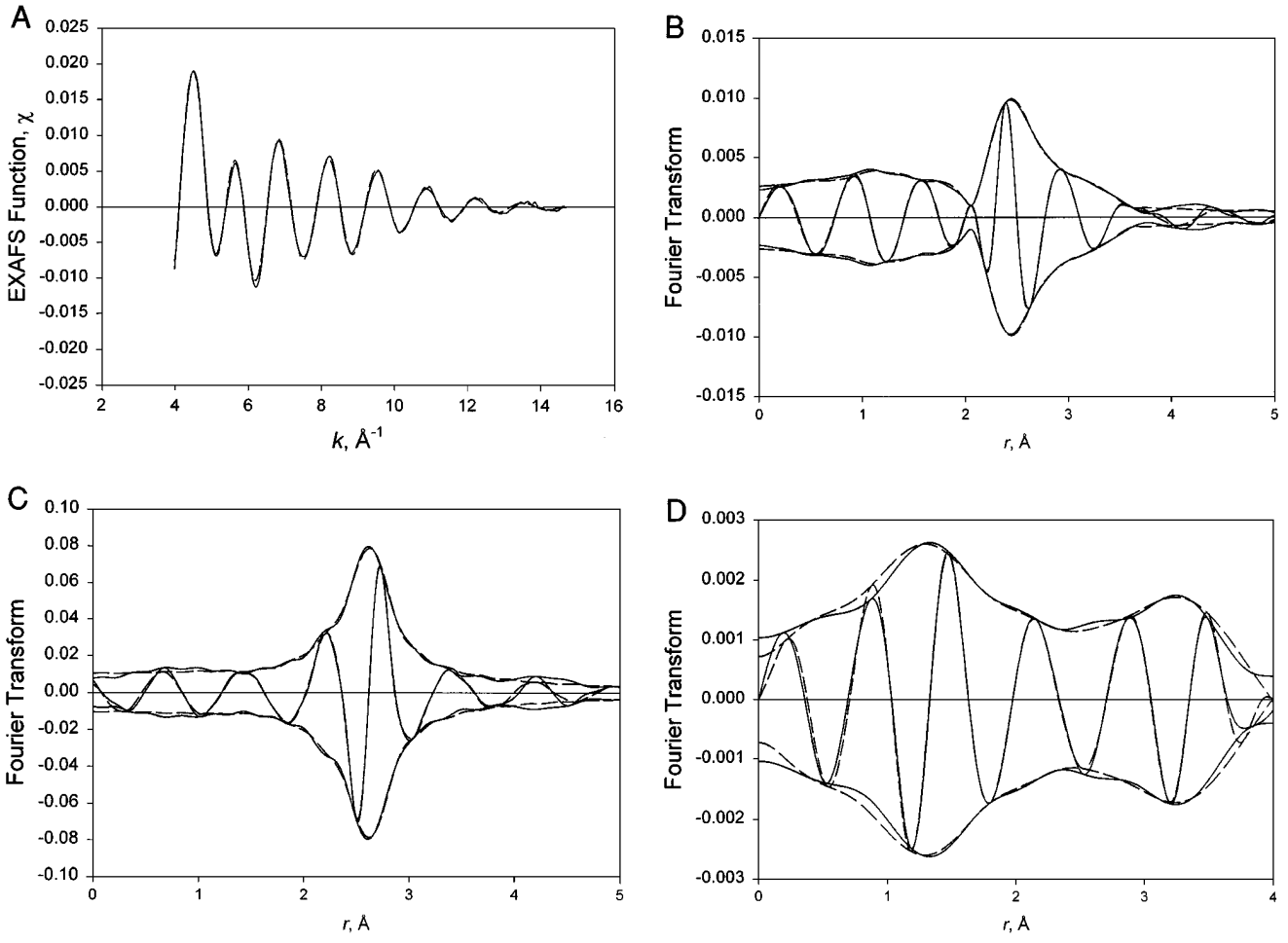

FIG. 1. Results of EXAFS analysis characterizing the sample formed by treatment of $[Rh_6(CO)_{16}]$ supported in NaY zeolite (calcined at 300°C) in H_2 at 250°C: (A) Raw EXAFS function (solid line) and sum of the calculated Rh–Rh + Rh–O_s + Rh–C + Rh–O* contributions (dashed line). (B) Imaginary part and magnitude of Fourier transform (unweighted, $\Delta k = 4.1$–14.6 Å^{-1}) of raw EXAFS function (solid line) and sum of the calculated Rh–Rh + Rh–O_s + Rh–C + Rh–O* contributions (dashed line). (C) Residual spectrum illustrating the Rh–Rh contribution; imaginary part and magnitude of Fourier transform (unweighted, Rh–Rh phase and amplitude corrected, $\Delta k = 4.1$–14.6 Å^{-1}) of raw EXAFS data minus calculated Rh–O_s + Rh–C + Rh–O* contributions (solid line) and calculated Rh–Rh contribution (dashed line). (D) Residual spectrum illustrating the Rh–low-*Z* interactions; imaginary part and magnitude of Fourier transform (unweighted, $\Delta k = 4.1$–10 Å^{-1}) of raw EXAFS data minus calculated Rh–Rh contribution (solid line) and calculated Rh–O_s + Rh–C + Rh–O* contributions (dashed line).

Rh K-edge XANES

The Rh *K*-edge XANES data characterizing the samples formed by treatment of $[Rh_6(CO)_{16}]$ in NaY zeolite (calcined at 300°C) in He or H_2 (Samples 3 and 6, Table 1) are shown in Fig. 2. Comparison of the data representing these two samples shows that the clusters formed in He at 300°C (Sample 3, Table 1) are more electron deficient than the aggregates formed in H_2 at 300°C (Sample 6, Table 1), as evidenced by the white-line intensities.

Toluene Hydrogenation Catalysis

Rhodium cluster catalysts. In a blank experiment with the reactor packed with only inert α-Al_2O_3 particles, the conversion of toluene and H_2 at 100°C and 1 atm was negligible. But when the toluene + H_2 mixture passed through a bed containing decarbonylated (Samples 1–3, Tables 1 and 2) or partially decarbonylated rhodium clusters (Sample 4), the effluent contained methylcyclohexane, indicating the occurrence of catalytic hydrogenation.

Each catalyst underwent slow deactivation following an induction period of about 2 h, as illustrated by the typical results of Fig. 3. The samples containing decarbonylated (Samples 1–3) or partially decarbonylated rhodium clusters (Sample 4) showed a steady deactivation over a period of about 4 days, after which the catalyst had lost about 90% of its initial activity. The reported rates were found by extrapolating the data to zero time on stream, excluding the induction period (Fig. 4). The rates were determined from differential conversions less than about 2%, and they are represented as turnover frequencies in units of [molecules of toluene converted (Rh atom · s)$^{-1}$] (Table 2). Evidence

TABLE 1

EXAFS Results Characterizing Rhodium Clusters Supported on NaY Zeolite or NaX Zeolite Formed by Decarbonylation of $[Rh_6(CO)_{16}]$ or $[Rh_6(CO)_{15}]^{2-}$, respectively, in He or H_2[a]

Zeolite support/ sample number	Support preparation conditions[b]			Conditions of sample treatment			EXAFS parameters[c,d]			
	Treatment gas	Temp. (°C)	Time (h)	Treatment gas	Temp. (°C)	Time (h)	N	R (Å)	$\Delta\sigma^2$ (Å^2)	ΔE_0 (eV)
NaY/1	O_2	300	4	He	200	2	3.8	2.68	0.00376	2.9
NaY/2	O_2	300	4	He	250	2	3.5	2.69	0.00399	4.1
NaY/3	O_2	300	4	He	300	2	3.9	2.68	0.00391	4.4
NaY/4	O_2	300	4	H_2	200	2	3.5	2.68	0.00445	6.6
NaY/5	O_2	300	4	H_2	250	2	4.6	2.68	0.00476	5.7
NaY/6	O_2	300	4	H_2	300	2	6.7	2.68	0.00348	5.3
NaX/7	—	25	—	He	200	2	2.6	2.65	0.00384	12.6
NaX/8	—	25	—	He	250	2	—	—	—	—
NaX/9	—	25	—	He	300	2	2.6	2.65	0.00423	7.2
NaX/10	—	25	—	H_2	200	2	3.6	2.69	0.00643	12.7
NaX/11	—	25	—	H_2	250	2	—	—	—	—
NaX/12	—	25	—	H_2	300	2	6.2	2.65	0.00422	5.0

[a] Notation. N, Rh–Rh coordination number; R, absorber (Rh)-backscatterer distance; $\Delta\sigma^2$, Debye–Waller factor; ΔE_0, inner potential correction.
[b] Samples evacuated at treatment temperature for 12 h (following gas treatment for samples treated in O_2).
[c] Details of EXAFS analysis and fitting of data characterizing NaY zeolite samples given elsewhere (15).
[d] Details of EXAFS analysis and fitting of data characterizing NaX zeolite samples given elsewhere (17).

that the conversions were differential is illustrated by the data of Fig. 5. The turnover frequencies were calculated on the basis of the assumption that all the rhodium atoms were surface atoms and therefore accessible. This assumption involves neglect of any blockage of rhodium atoms by the support.

The apparent activation energies determined from the temperature dependencies of the turnover frequencies (Fig. 6) were found to be about 11 kcal/mol for catalysis by the fully decarbonylated rhodium clusters (Samples 2 and 3, Tables 1 and 2), whereas the value was found to be about 5 kcal/mol for catalysis by partially decarbonylated clusters formed in H_2 (Samples 4 and 10, Tables 1 and 2) or the almost fully decarbonylated clusters formed in He (Sample 1, Tables 1 and 2).

Rhodium aggregate catalysts. The supported rhodium aggregates (Sample 5 and 6, Tables 1 and 2) were found to be more active catalytically than the supported clusters. The values in Table 2 are reported per total Rh atom; thus the rates characterizing the rhodium aggregates are not turnover frequencies because not all the Rh atoms were surface atoms, as shown by the EXAFS results (Table 1). Therefore, this comparison of the clusters and aggregates

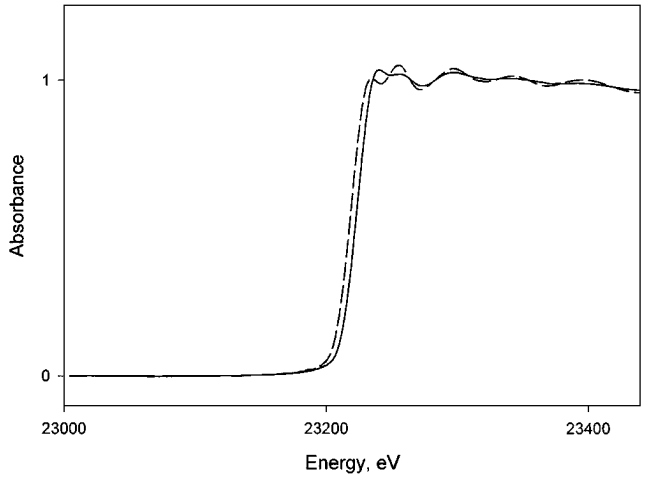

FIG. 2. XANES characterizing NaY zeolite-supported sample formed from $[Rh_6(CO)_{16}]$ treated in He at 200°C (to give rhodium clusters) (solid line) or in H_2 at 300°C (to give rhodium aggregates) (dashed line).

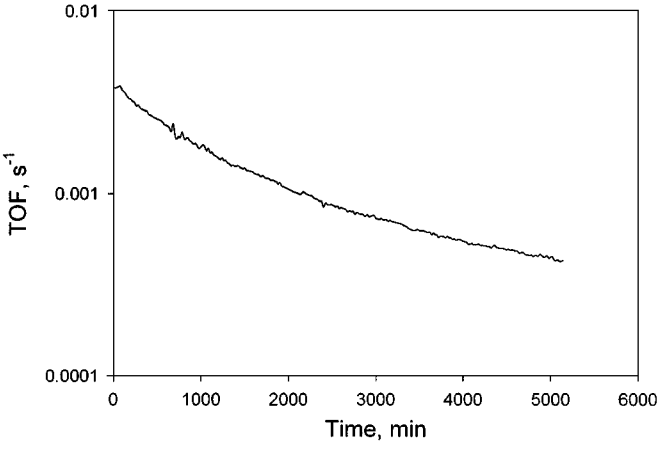

FIG. 3. Toluene hydrogenation catalyzed by rhodium clusters formed by treatment of $[Rh_6(CO)_{16}]$ supported in NaY zeolite (calcined at 300°C) in H_2 at 250°C. Reaction conditions: $P_{toluene} = 50$ Torr, $P_{H_2} = 710$ Torr, temperature = 80°C.

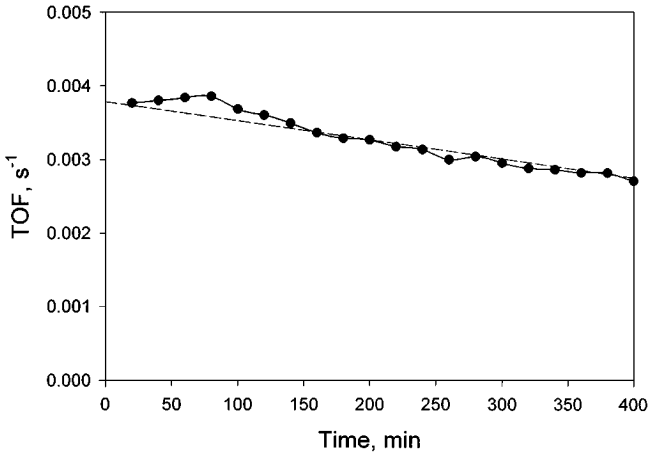

FIG. 4. Toluene hydrogenation catalyzed by rhodium clusters formed by treatment of $[Rh_6(CO)_{16}]$ supported in NaY zeolite (calcined at 300°C) in H_2 at 250°C showing reaction rate at time on stream of zero. Reaction conditions: $P_{toluene} = 50$ Torr, $P_{H_2} = 710$ Torr, temperature = 80°C.

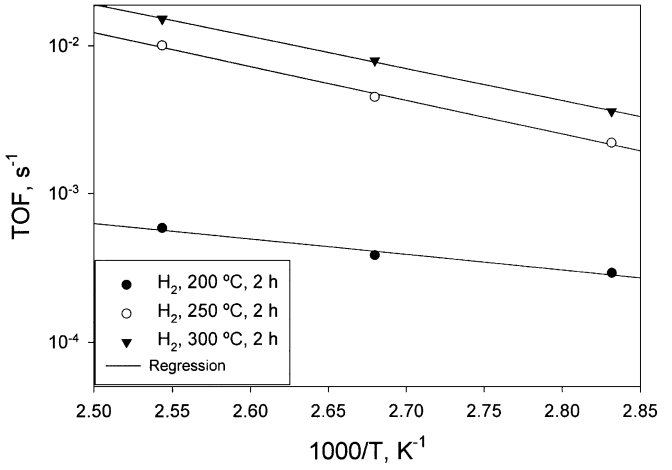

FIG. 6. Arrhenius plot for toluene hydrogenation catalyzed by rhodium clusters formed by treatment of $[Rh_6(CO)_{16}]$ supported in NaY zeolite (calcined at 300°C) in H_2 at 200 (closed circles), 250 (open circles), or 300°C (triangles). Reaction conditions: $P_{toluene} = 50$ Torr, $P_{H_2} = 710$ Torr; total feel flow rate, 46 ml (NTP)/min; catalyst mass = 40 mg, Rh content of catalyst, 2.3 wt%.

understates the difference in their activities per exposed Rh atom. Because all the catalysts had high rhodium dispersions [a Rh–Rh first-shell coordination number of about 7 corresponds to a dispersion of about 80% (26)], it follows that a comparison based on turnover frequencies would not lead to a significantly different conclusion from that just stated. Thus, the data show that the aggregates (Samples 5 and 6, Table 2) are characterized by turnover frequencies at least an order of magnitude greater than those of the decarbonylated (Samples 2 and 3) or partially decarbonylated rhodium clusters (Samples 1 and 4, Table 2).

The apparent activation energies of the reaction catalyzed by the rhodium aggregates are approximately equal to the apparent activation energies of the reaction catalyzed by the fully decarbonylated rhodium clusters. These values are nearly twice that characteristic of the reaction catalyzed by the partially or nearly fully decarbonylated clusters—and the low values characteristic of the less than fully decarbonylated clusters might be evidence of an intraparticle transport limitation related to blockage of the pores by the relatively large $[Rh_6(CO)_{16}]$ molecules.

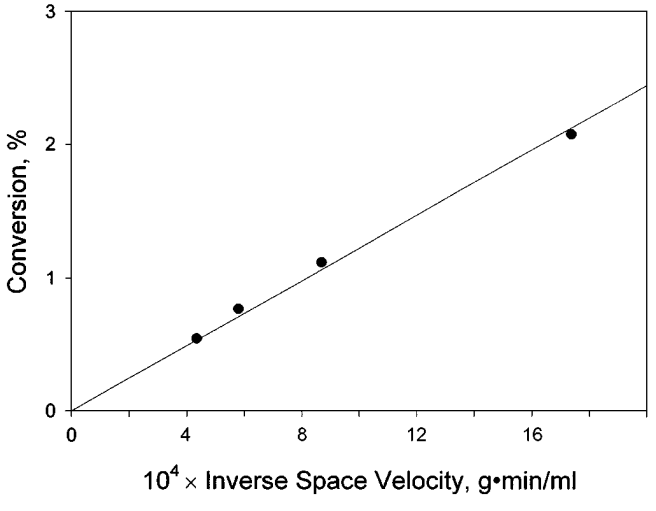

FIG. 5. Differential conversion of toluene catalyzed by rhodium clusters formed by treatment of $[Rh_6(CO)_{16}]$ supported in NaY zeolite (calcined at 300°C) in H_2 at 250°C. Reaction conditions: $P_{toluene}/P_{H_2} = 50/710$, temperature = 80°C.

EXAFS Spectra of Used Catalysts

Used, nearly fully decarbonylated cluster catalysts. The raw EXAFS data characterizing the nearly fully decarbonylated rhodium clusters that had been used as catalysts at 100°C for 4 h (Sample 1, Table 2) show oscillations up to values of k equal to about 16 $Å^{-1}$, consistent with Rh–Rh contributions. Because the used catalyst formed by the treatment of supported $[Rh_6(CO)_{16}]$ in He at 200°C is expected [on the basis of a lack of significant ν_{CO} bands (15)] to have incorporated few if any CO ligands, a Rh–O* contribution was not fitted. However, an additional Rh–O contribution (without multiple scattering) was fitted, at about 2.9 Å. The used catalyst was characterized by a Rh–Rh first-shell coordination number of 3.4 (Table 3), which is indistinguishable from that of the precursor (3.2).

Used, partially decarbonylated cluster catalysts. The EXAFS data characterizing the partially decarbonylated rhodium clusters (Sample 4, Table 2), after catalysis at 100°C for 4 h, show oscillations up to values of k equal to about 16 $Å^{-1}$, consistent with Rh–Rh contributions (Fig. 7A). The averaged data were fitted satisfactorily by a Rh–Rh contribution, at 2.69 Å, and Rh–low-Z contributions, approximated as a short Rh–O (2.1 Å), a Rh–O*

TABLE 2

Toluene Hydrogenation Catalyzed by Rhodium and Iridium Clusters Supported in NaY Zeolite and NaX Zeolite

Zeolite support/ sample number[a]	N_{Rh-Rh}	Approximate cluster nuclearity[b]	Reaction temperature (°C)	$10^4 \times$ TOF (s^{-1})	Apparent activation energy (kcal/mol)	H/Rh from chemisorption data
NaY/1	3.8	6	80	0.8	5.1	0.16
			100	1.0		
			120	1.7		
NaY/2	3.5	6	80	2.1	11.5	0.15
			100	5.0		
			120	11		
NaY/3	3.9	6	80	1.0	13.8	0.17
			100	3.0		
			120	7.5		
NaY/4	3.5	6	80	2.9	4.8	0.10
			100	3.8		
			120	5.8		
NaY/5	4.6	6–10	80	43	9.1	0.40
			100	85		
			120	160		
NaY/6	7.5	50	80	36	9.9	0.45
			100	79		
			120	150		
NaX/7	2.6	≤6	80	3.0	10.4	0.12
			100	9.0		
			120	13		
NaX/8	—	≤6	80	2.8	11.7	0.11
			100	10		
			120	15		
NaX/9	2.6	≤6	80	3.0	11.6	0.15
			100	9.0		
			120	16		
NaX/10	3.6	6	80	0.7	5.0	0.14
			100	1.1		
			120	1.4		
NaX/11	—	6–10	80	2.4	7.9	0.16
			100	4.3		
			120	7.5		
NaX/12	6.2	20	100	70	—	0.39
NaY[c]		6	60	2.5[d]	11.2[d]	—

[a] See Table 1.
[b] See Ref. (27).
[c] Ref. (2); catalyst sample contains NaY zeolite-supported Ir_6 clusters formed from $[Ir_6CO_{16}]$.
[d] Reactant partial pressures were the same as in this work.

(3.0 Å), and a Rh–C contribution (1.95 Å) (Table 3). These results are consistent with the infrared data (15) showing that the CO ligands were not completely removed at 200°C in H_2, as the catalytic reaction took place at lower temperatures and a lower H_2 partial pressure than those used in the partial decarbonylation process. The used catalyst is characterized by a Rh–Rh first-shell coordination number of 3.9, which is barely distinguishable from that of the precursor (3.2) within the expected error (Fig. 7B).

Characterization of Decarbonylated Rhodium Clusters by Hydrogen Chemisorption

The data representing chemisorption of hydrogen on supported rhodium clusters and aggregates are summarized in Table 2. The amount of hydrogen chemisorbed per Rh atom of the clusters formed by decarbonylation in He (Samples 1–3) was nearly the same for each sample, just as the Rh–Rh first-shell coordination numbers were nearly the same

TABLE 3

EXAFS Results Characterizing Rhodium Clusters Supported on NaY Zeolite or NaX Zeolite Formed by Decarbonylation of $[Rh_6(CO)_{16}]$ or $[Rh_6(CO)_{15}]^{2-}$, Respectively, in He or H_2, and Subsequently Used to Catalyze Toluene Hydrogenation[a]

Zeolite support/ sample number	Support preparation conditions[b]			Conditions of treatment of sample			EXAFS parameters[c]			
	Treatment gas	Temp. (°C)	Time (h)	Treatment gas	Temp. (°C)	Time (h)	N	R (Å)	$\Delta\sigma^2$ (Å^2)	ΔE_0 (eV)
NaY/1	O_2	300	4	He	200	2	3.4	2.66	0.00433	2.2
NaY/4	O_2	300	4	H_2	200	2	3.9	2.67	0.00482	6.9
NaX/10	—	25	—	H_2	200	2	3.7	2.71	0.00665	17.8
NaX/12	—	25	—	H_2	300	2	6.2	2.65	0.00422	5.0

[a] Notation as in Table 1.
[b] Samples were evacuated at treatment temperature for 12 h (following gas treatment for samples treated in O_2).
[c] Results of EXAFS analysis and fitting of data characterizing NaX zeolite samples given elsewhere (17).

for these samples (Table 2). The amount of irreversibly adsorbed hydrogen per Rh atom increased with increasing decarbonylation temperature when the samples were decarbonylated in H_2—as the decarbonylation temperature increased, the amount of adsorbed CO decreased and the average cluster or aggregate size increased. The data representing the (almost) fully decarbonylated samples (Samples 1–3 and 6) show that the H/Rh ratio increased with increasing cluster or aggregate size indicated by the EXAFS data (Table 2). A comparison of the results characterizing the decarbonylated clusters (Samples 1–3) with those characterizing the partially decarbonylated clusters (Sample 4) shows less hydrogen uptake on the latter, consistent with the presence of CO.

DISCUSSION

Metal Clusters in Faujasites

The Rh–Rh first-shell coordination number of the clusters formed by decarbonylating the zeolite-supported sample containing predominantly $[Rh_6(CO)_{16}]$ in He at 300°C (3.5) was approximately the same as that of pure $[Rh_6(CO)_{16}]$ (4.0) and that of the sample containing this precursor (3.2). This comparison indicates that the preparation was successful in giving small rhodium clusters that were not much different in nuclearity, on average, from the precursor. Thus, the best-prepared sample is modeled rather well as supported Rh_6, although it was not exclusively Rh_6, just as the precursor was not exclusively $[Rh_6(CO)_{16}]$.

As shown elsewhere (17), when uncalcined NaX zeolite was used instead of NaY zeolite, rhodium clusters having few if any CO ligands were formed by treatment of the samples that initially contained largely $[Rh_6(CO)_{15}]^{2-}$; the decarbonylation treatment was in He at 200, 250, or 300°C. The Rh–Rh first-shell coordination numbers characterizing the clusters in these samples were only about 2.6 (Table 1, Samples 6 and 8) (17). The low Rh–Rh first-shell coordination numbers characterizing the decarbonylated clusters relative to that of the precursor rhodium carbonyls (3.6) are consistent with the formation of raft-like structures or highly distorted octahedra (17); it is also possible that the clusters in NaX zeolite fragmented when decarbonylated.

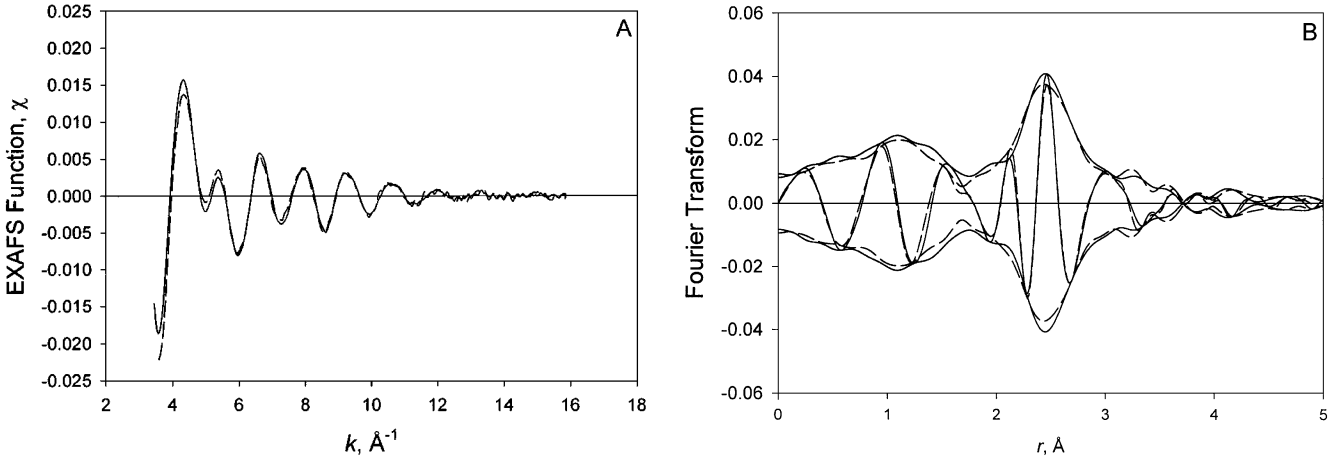

FIG. 7. Comparison of the X-ray absorption data characterizing rhodium clusters formed by treatment of $[Rh_6(CO)_{16}]$ supported in NaY zeolite (calcined at 300°C) treated in H_2 at 200°C prior to catalysis (solid line) and after catalysis (dashed line). (A) Raw EXAFS functions. (B) Imaginary part and magnitude of Fourier transform (unweighted, $\Delta k = 4.1$–14.6 Å^{-1}) of raw EXAFS functions.

The results for each of the rhodium-in-zeolite samples parallel those of Kawi *et al.* (3), who decarbonylated NaY zeolite-supported $[Ir_6(CO)_{16}]$ to form clusters that were modeled as predominantly Ir_6.

These metal-in-zeolite samples provide opportunities to compare (a) the catalytic activities of rhodium and iridium clusters of nearly the same size on the same support and (b) the activities of supported rhodium clusters of nearly the same size on different supports. However, the data do not allow the most fundamental comparison of the effects of the support or the metal, because the metals in the zeolites might have been distributed nonuniformly in the supports and because the transport of reactants and products in the narrow zeolite pores might have influenced the catalytic reaction rates. The evidence is as follows:

(1) The uncalcined NaY zeolite sample containing $[Rh(CO)_2(acac)]$ was darker gray than the calcined NaY zeolite sample containing $[Rh(CO)_2(acac)]$. Furthermore, carbonylation of the former gave a higher yield of $[Rh_6(CO)_{16}]$ than carbonylation of the latter, and the former decarbonylated sample was darker than the latter. These results suggest that the distributions of rhodium in the two zeolites were different; we suggest the rhodium in the uncalcined zeolite was concentrated near the crystallite surfaces.

(2) Decarbonylation of these samples in He at 200°C gave rhodium aggregates in the uncalcined zeolite characterized by a Rh–Rh first-shell coordination number of about 7 (15) and gave rhodium clusters in the calcined zeolite characterized by a Rh–Rh first-shell coordination number only 3.3. Thus, we infer that the clusters formed in the former were less resistant to aggregation than those formed in the latter, and the resistance to aggregation is correlated with the concentration gradient of the rhodium-containing precursors suggested in the preceding paragraph. The degree of aggregation of the rhodium in the decarbonylated samples might be explained in terms of the local concentration of the precursors in the zeolite pores or the water content of the zeolite.

(3) The extent of aggregation of rhodium in the uncalcined zeolites varied from sample to sample, whereas rhodium in the calcined zeolites was always stable to aggregation under mild conditions (15, 27).

(4) The Thiele modulus for toluene hydrogenation catalyzed by NaY zeolite-supported rhodium clusters is estimated (27) to be about 0.2, whereas the value for the supported rhodium aggregates is estimated to be about 2 (27). We stress that these estimates are rough. These estimates imply that the intraparticle transport influence was almost negligible (the effectiveness factor was nearly 1) when toluene hydrogenation was catalyzed by clusters and that the effectiveness factor was only slightly less (roughly 0.8) when the reaction was catalyzed by the aggregates.

Stability of Supported Clusters during Catalysis

The EXAFS data characterizing the used and unused supported cluster catalysts show that they were stable during catalysis. Thus, the comparisons of the catalysts based on the EXAFS parameters representing the fresh catalysts are well founded.

Similarly, because the Rh–Rh first-shell coordination numbers characterizing fresh and used clusters in NaX zeolite were nearly equal (17, 27), we infer that these clusters were also stable during catalysis.

Toluene Hydrogenation Catalyzed by Supported Clusters

Thus, we have the opportunity to compare the performance of rhodium clusters of nearly the same size as catalysts supported in zeolites with the same framework structure and different compositions, NaY and NaX. Furthermore, because iridium clusters consisting of approximately 6 atoms each, on average, have also been synthesized in NaY zeolite, we have the opportunity to compare the activities of rhodium and iridium clusters of nearly the same size in the same support, NaY zeolite. We emphasize, however, that the caveats stated above related to mass transport and nonuniform distribution of metal in the zeolites apply to all these samples, making the comparisons of the properties of rhodium and iridium clusters less fundamentally sound than one would ideally prefer.

Near lack of support effect. The data (Table 2) show that the activities varied by a factor of only about 2 as the support changed from NaY to NaX zeolite. We regard these activities as indistinguishable from each other within the expected errors. The important conclusion is that the support effect is small.

The apparent activation energies characterizing the reaction in the presence of the zeolite-supported rhodium catalysts (Table 2) are indistinguishable from each other within experimental error, consistent with the nearly equal activities referred to in the preceding paragraph. The results thus suggest that the influence of intracrystalline mass transport may not have been significant in these catalysts, in agreement with the rough estimates of effectiveness factors stated above. These apparent activation energies are similar to those observed for reaction catalyzed by supported platinum (28); we might thus suggest that the mechanism of toluene hydrogenation on the supported rhodium clusters is similar to that on larger metal aggregates, with the rate limiting step being the first insertion of hydrogen.

Effect of cluster size on catalytic activity. Lin and Vannice (29, 30) presented data indicating that the hydrogenation of arenes catalyzed by supported platinum is structure insensitive. Boudart and Sajkowski (31) presented data indicating that hydrogenation of cyclohexene catalyzed by supported rhodium is structure insensitive—the turnover

frequencies for reactions catalyzed by supported rhodium clusters or aggregates having Rh–Rh first-shell coordination numbers of about 5 or greater were independent of the cluster or aggregate size and the support. However, the clusters or aggregates investigated by these researchers were larger on average than the clusters investigated in this work (Samples 1–3), and size effects may become important for the smallest clusters, even for structure-insensitive reactions (2, 32). The rhodium supported in NaY zeolite or NaX zeolite shows a strong dependence of turnover frequency on cluster or aggregate size. The activities of decarbonylated rhodium clusters are much less than those of rhodium aggregates (Samples 5 and 6) (Table 2).

The cluster/aggregate size issues are complex and unexplained (32). As the XANES data show that the clusters are somewhat electron deficient, it seems plausible to suggest that differences in catalytic activity between supported metal clusters and aggregates may be a consequence of the support's role in withdrawing electron density from the clusters, rather than simply an effect of cluster size.

Comparison of catalytic activities of supported rhodium and iridium clusters. Data characterizing the activities of clusters approximated as Ir_6 in NaY zeolite have been reported (2). Because the conditions of the rate measurement made for clusters of iridium in NaY zeolite almost overlap the conditions of the rate measurements made in this work, they provide an opportunity to determine the effect of a change in the metal on catalytic properties—without substantial changes in the support or the metal cluster size.

The activities of the iridium clusters in NaY zeolite for toluene hydrogenation at 60°C (2) are slightly greater than those of supported rhodium clusters in the same zeolite measured at 80°C. The apparent difference may be indistinguishable from the errors in the data, and more results are needed to bolster the comparison.

CONCLUSIONS

Rhodium clusters were formed in NaY zeolite cages by decarbonylation of $[Rh_6(CO)_{16}]$. Treatment in He gave decarbonylated clusters with metal frames about as small as those of the precursor, and treatment in H_2 at 200°C gave only partially decarbonylated clusters with nearly the same metal frame. The rhodium clusters in NaY zeolite are catalytically active for toluene hydrogenation, with the activity being nearly the same as that of rhodium clusters of almost the same size in NaX zeolite, demonstrating that the support effect is small. The supported rhodium clusters are markedly less active than larger rhodium aggregates and similar in activity to supported iridium clusters of nearly the same size.

ACKNOWLEDGMENTS

The research was supported by the U. S. Department of Energy, Office of Energy Research, Office of Basic Energy Sciences, Division of Chemical Sciences, Contract FG02-87ER13790. We acknowledge the support of the U. S. Department of Energy, Division of Materials Sciences, under Contract DE-FG05-89ER45384, for its role in the operation and development of beam line X-11A at the National Synchrotron Light Source (NSLS). The NSLS is supported by the Department of Energy, Division of Materials Sciences and Division of Chemical Sciences, under Contract DE-AC02-76CH00016. We thank the staff of beam line X-11A for their assistance. We also acknowledge the Stanford Synchrotron Radiation Laboratory for access to beam time. X-ray absorption data were analyzed with the XDAP software (33).

REFERENCES

1. *Oil Gas J.* **190**, 29 (1992).
2. Xu, Z., Xiao, F.-S., Purnell, S. K., Alexeev, O., Kawi, S., Deutsch, S. E., and Gates, B. C., *Nature (London)* **372**, 346 (1994).
3. Kawi, S., Chang, J.-R., and Gates, B. C., *J. Phys. Chem.* **97**, 5375 (1993).
4. Maloney, S. D., van Zon, F. B. M., Kelley, M. J., Koningsberger, D. C., and Gates, B. C., *Catal. Lett.* **5**, 161 (1990).
5. van Zon, F. B. M., Maloney, S. D., Gates, B. C., and Koningsberger, D. C., *J. Am. Chem. Soc.* **115**, 10,317 (1993).
6. Xu, Z., Rheingold, A. L., and Gates, B. C., *J. Phys. Chem.* **97**, 9465 (1993).
7. Lamb, H. H., Fung, A. S., Tooley, P. A., Puga, J., Krause, T. R., Kelley, M. J., and Gates, B. C., *J. Am. Chem. Soc.* **111**, 8367 (1989).
8. Liu, A.-M., Shido, T., and Ichikawa, M., *J. Chem. Soc. Chem. Commun.* 507 (1995).
9. Zhao, A., and Gates, B. C., *J. Am. Chem. Soc.* **118**, 2458 (1996).
10. Zhao, A., and Gates, B. C., *J. Catal.* **168**, 60 (1997).
11. Kawi, S., Chang, J.-R., and Gates, B. C., *J. Catal.* **142**, 585 (1993).
12. Gates, B. C., *Chem. Rev.* **95**, 511 (1995).
13. Somerville, D. M., Nashner, M. S., Nuzzo, R. G., and Shapley, J. R., *Catal. Lett.* **46**, 17 (1997).
14. Jentoft, R. E., Deutsch, S. E., and Gates, B. C., *Rev. Sci. Instrum.* **67**, 2111 (1996).
15. Weber, W. A., and Gates, B. C., *J. Phys. Chem. B* **101**, 10,423 (1997).
16. Duivenvoorden, F. B. M., Koningsberger, D. C., Uh, Y. S., and Gates, B. C., *J. Am. Chem. Soc.* **108**, 6254 (1986).
17. Weber, W. A., and Gates, B. C., to be published.
18. Shannon, R. D., Vedrine, J. C., Naccache, C., and Lefebvre, R., *J. Catal.* **88**, 431 (1988).
19. Hanson, B. E., Davis, M. E., Taylor, D., and Rode, E., *Inorg. Chem.* **23**, 52 (1984).
20. Lefebvre, F., and Ben Taarit, Y., *Nouv. J. Chim.* **8**, 387 (1984).
21. Wong, T. T., Zhang, Z., and Sachtler, W. M. H., *Catal. Lett.* **4**, 365 (1990).
22. Rao, L.-F., Fukuoka, A., Kosugi, N., Kuroda, H., and Ichikawa, M., *J. Phys. Chem.* **94**, 5317 (1990).
23. Mantovani, E., Palladino, N., and Zanobi, A., *J. Mol. Catal.* **3**, 285 (1977/8).
24. Davis, M. E., Rode, E. J., Taylor, D., and Hanson, B. E., *J. Catal.* **86**, 67 (1984).
25. Rode, E. J., Davis, M. E., and Hanson, B. E., *J. Catal.* **96**, 574 (1985).

26. Kip, B. J., Duivenvoorden, F. B. M., Koningsberger, D. C., and Prins, R., *J. Catal.* **105**, 26 (1987).
27. Weber, W. A., Ph.D. Dissertation, University of California, Davis, 1998.
28. Lin, S. D., and Vannice, M. A., *J. Catal.* **143**, 563 (1993).
29. Lin, S. D., and Vannice, M. A., *J. Catal.* **143**, 539 (1993).
30. Lin, S. D., and Vannice, M. A., *J. Catal.* **143**, 554 (1993).
31. Boudart, M., and Sajkowski, D. J., *Faraday Discuss. Chem. Soc.* **92**, 57 (1991).
32. Xiao, F.-S., Weber, W. A., Alexeev, O., and Gates, B. C., *in* "Proceedings, 11th International Congress on Catalysis" (J. W. Hightower, W. N. Delgass, E. Iglesia, and A. T. Bell, Eds.), p. 1135. Elsevier, Amsterdam, 1996.
33. Vaarkamp, M., Linders, J. C., and Koningsberger, D. C., *Physica B* **209**, 159 (1995).